Reduction of Spin Injection Efficiency by Interface Defect Spin Scattering in ZnMnSe/AlGaAs-GaAs Spin-Polarized Light-Emitting Diodes

R. M. Stroud, A. T. Hanbicki, Y. D. Park,* G. Kioseoglou, A. G. Petukhov,† and B. T. Jonker
Naval Research Laboratory, Washington, D.C. 20375

G. Itskos and A. Petrou
State University of New York at Buffalo, Buffalo, New York 14260
(Received 24 October 2001; published 26 September 2002)

We report the first experimental demonstration that interface microstructure limits diffusive electrical spin-injection efficiency across heteroepitaxial interfaces. An inverse correlation between spin-polarized electron injection efficiency and interface defect density is demonstrated for ZnMnSe/AlGaAs-GaAs spin-polarized light-emitting diodes that exhibit quantum well spin polarizations up to 85%. A theoretical treatment shows that the suppression of spin injection due to interface defects results from the contribution of the defect potential to the spin-orbit interaction, which increases the spin-flip scattering.

DOI: 10.1103/PhysRevLett.89.166602 PACS numbers: 72.25.Hg, 61.72.Dd, 72.25.Mk, 72.25.Rb

Electrical injection of spin-polarized electrons across a heteroepitaxial interface into a semiconductor has been demonstrated for all-semiconductor systems, in which electron spin polarizations of 50%–85% were directly measured [1,2]. The substantially larger effects observed for the all-semiconductor systems, as compared to ferromagnetic metal/semiconductor (0.1% to 1%) [3] and ferromagnetic metal/tunnel barrier/semiconductor systems (2%–13%) [4], may be due to better conductivity [5] and band matching [6] and the ability to grow isostructural interfaces [7]. However, the extent to which the interface microstructure limits polarized injection efficiency, and spintronic device performance, is not known.

We have studied the effects of the interface microstructure on spin-injection efficiency in $Zn_{1-x}Mn_xSe/Al_yGa_{1-y}As$-GaAs spin-polarized light-emitting diodes (spin-LEDs) (Fig. 1). In this device [8], spin-polarized electrons are injected from the ZnMnSe into the GaAs quantum well (QW), where radiative recombination of the carriers results in the emission of circularly polarized light. The quantum selection rules relate the circular polarization of the light emitted along the surface normal to the spin polarization of the carriers involved [9]. The spin-LED thus provides a quantitative, model-independent measure of the electron spin polarization produced in the QW by electrical injection and, thereby, an indication of the spin-injection efficiency [2]. We show that the QW spin polarization correlates inversely with the density of linear defects resulting from stacking faults at the ZnMnSe/AlGaAs interface. This correlation is explained by a model that incorporates spin-orbit (Elliot-Yafet) scattering and shows that the asymmetric potential of the interface defect results in strong spin-flip scattering in the forward direction. These results provide the first experimental demonstration that interface defect structure limits spin-injection efficiency in the diffusive transport regime, in which all existing electronic devices operate. Because linear interface defects associated with stacking faults occur in all cubic heteroepitaxial systems, these defects are a potential source of spin polarization loss for semiconductor spintronic devices in general.

Samples were grown by molecular beam epitaxy in a multichamber system [2]. The growth was initiated with a 1 μm p-type GaAs buffer layer on semi-insulating GaAs (001) substrates, followed by the LED (50 nm p-doped $Al_{0.1}Ga_{0.9}As$, 15 nm GaAs quantum well, 50 nm n-doped $Al_{0.1}Ga_{0.9}As$), the n-$Zn_{0.94}Mn_{0.06}Se$ injector, and in some cases an n^+ZnSe contact layer. The use of a 15 nm GaAs quantum well lifts the heavy hole/light hole band degeneracy. The density of defects at the ZnMnSe/AlGaAs interface was crudely controlled by varying the net thickness of the II-VI layers.

The samples were patterned into surface-emitting LEDs 200 to 400 μm in diameter using standard photolithography and chemical etching techniques. The spin-injection efficiency was assessed by measuring the

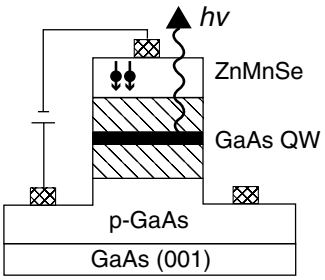

FIG. 1. Schematic of the ZnMnSe/AlGaAs-GaAs spin-LED. Spin-polarized electrons are injected across the ZnMnSe-AlGaAs interface into the GaAs quantum well. Radiative recombination in the QW results in circularly polarized light emission.

circular polarization of the GaAs heavy hole free exciton in the Faraday geometry using a quarter wave plate followed by a linear polarizer and spectrometer. In this configuration, the circular polarization is equal to the electron spin polarization in the QW [2] and, thus, provides a direct measure of the spin polarization due to electrical injection from the ZnMnSe contact. These measurements were made at 4.2 K with fields up to 8 T. Further experimental details may be found elsewhere [2].

The defect density was determined from dark-field [$g = (2\bar{2}0)$] transmission electron imaging of [$1\bar{1}0$] cross sections. The most prevalent defects observed were stacking faults (SFs) in $\langle 111 \rangle$ directions, nucleating at or near the ZnMnSe-AlGaAs interface. No secondary phases, Mn clusters, or defects in the AlGaAs-GaAs LEDs were found. The SFs appear in dark-field images as diagonal lines extending from the heterointerface to the ZnMnSe film surface (Fig. 2). The number density of these SFs was determined from a series of dark-field images by counting the SFs per unit length along the [110] direction. An equivalent number of such defects lie in the perpendicular direction, but are not visible in this cross section. These SFs are a well-known problem in ZnSe/GaAs epitaxy [10] and are attributed to both lattice strain [11] and the formation of Se dimers at the interface [12]. Away from the immediate vicinity of a SF, high-resolution lattice images reveal a structurally well-ordered interface.

The electron spin polarization in the GaAs QW of the spin-LEDs correlates inversely with the observed SF density, as shown in Fig. 3. This correlation clearly demonstrates a link between the injection efficiency and interface microstructure. It is remarkable to note that spin-injection efficiencies leading to QW spin polarizations as high as 85% can be realized across the II-VI/III-V heterointerface despite moderately high (10^4–10^5 cm^{-1}) SF densities, attesting to the robust nature of the spin-injection process.

To theoretically analyze the relationship between spin polarization and defects, we have adapted a model of the scattering properties of defects with nonspherical symmetry that includes spin-orbit interactions. In principle, spin-flip scattering in the ZnMnSe can occur anywhere along the extended planar SFs. However, Oestreich *et al.* [13] have noted that in a semimagnetic semiconductor such as ZnMnSe, the minority spin lifetime is exceedingly short on the time scale of diffusive transport when the conduction band edge is split by a sufficiently large magnetic field. If a spin-flip scattering event occurs far above the ZnMnSe/AlGaAs interface, the carrier spin quickly relaxes to the majority spin channel before reaching the interface and being injected. Therefore, the relevant spin scattering in the spin-LED occurs at the interface, and we need consider only scattering from the line defect associated with the intersection of each SF plane with the interface plane (Fig. 4). These line defects lie in the interface plane and extend along the [110] and [$1\bar{1}0$] directions, referred to as the defect axes. The density of such line defects is simply equal to twice the SF density observed in the [$1\bar{1}0$] cross section as defined above.

The spin-orbit Hamiltonian associated with a lattice defect can be written from Kane's model as [14]:

$$H_{\mathrm{SO}} = \frac{\hbar\Delta}{3mE_g^2}\vec{\sigma}[\vec{\nabla}U(\vec{r}) \times \vec{p}], \tag{1}$$

where Δ is the spin-orbit splitting in the valence band, E_g is the band gap, m is the effective mass, $\frac{\hbar}{2}\vec{\sigma}$ is the spin operator, $\vec{p}$ is the momentum operator, and $U(\vec{r})$ is the potential of the defect. The Hamiltonian (1) is responsible

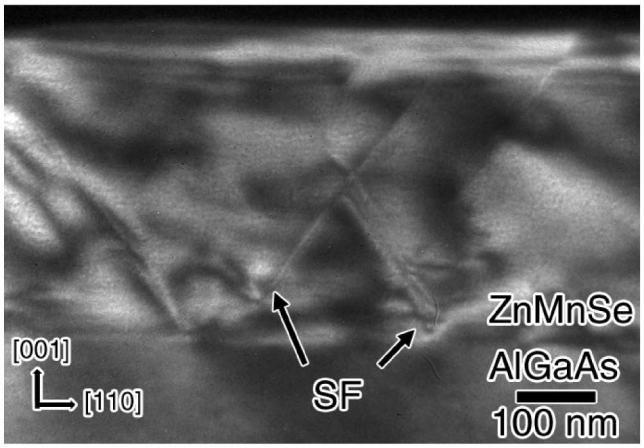

FIG. 2. Dark-field cross-sectional transmission electron micrograph of a ZnMnSe spin-LED. Stacking faults in $\langle 111 \rangle$ directions are observed to nucleate at the ZnMnSe-AlGaAs interface. This sample had a stacking fault concentration of 9×10^4 cm^{-1} and spin-injection efficiency of 49%.

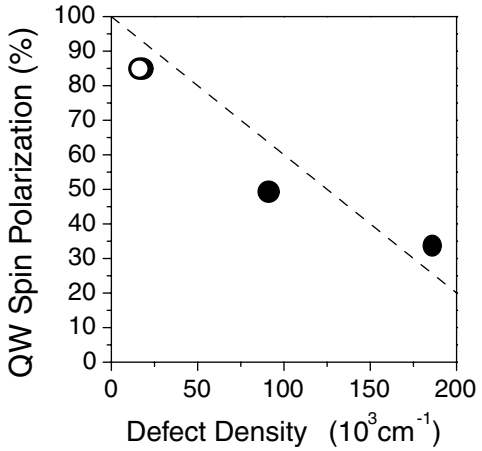

FIG. 3. Correlation of quantum well (QW) spin polarization with stacking fault density. Two data points nearly overlap at 85% polarization. The error bars are comparable to the symbol size. The dashed line is the calculated result from Eq. (5) and has no adjustable parameters.

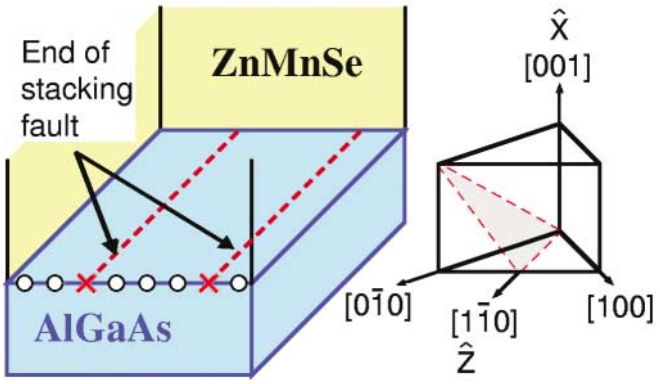

FIG. 4 (color). Diagram illustrating the linear interface defects resulting from the intercept of (111)-type SF planes and the interface plane. Only one of the four possible (111)-type SF planes is shown for clarity.

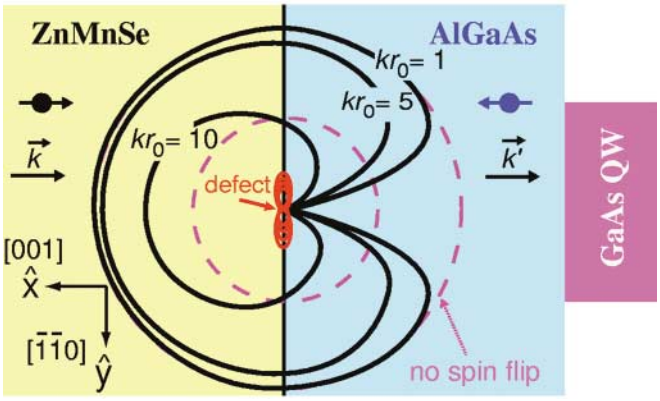

FIG. 5 (color). Angular distributions of the spin polarization about the axis of the linear interface defect (the [110] direction) for different values of kr_0 following scattering from the defect. The outer dashed circle corresponds to 100% spin polarization, while the inner circle divides the regions of the negative and positive polarizations. The dipole moment is oriented along the [110] direction, i.e., in the interface plane. Spin-flip scattering dominates for all electrons in the forward direction (towards the GaAs quantum well).

for the Elliot-Yafet spin-scattering mechanism in bulk III-V or II-VI semiconductors [14].

The potential for the line defect associated with the intersection of the stacking fault with the interface plane described above can be written [15]:

$$U(\vec{r}) = (A/\rho) f(\rho) \sin\varphi, \tag{2}$$

where the conventional polar coordinate system is used with the x, y, and z axes chosen along the [001], [$\bar{1}\bar{1}$0], and [1$\bar{1}$0] directions, respectively (see Figs. 4 and 5). This potential describes a line dipole with the defect axis along [1$\bar{1}$0] and the dipole moment parallel to the [110] axis. The distance from a probe point to the axis of the linear defect is ρ, φ is the azimuthal angle, $f(\rho)$ is a Thomas-Fermi screening function such that $f(0) = 1$ and $f(\infty) = 0$, and A is a constant combining several material parameters such as deformation potential, dielectric constant, and the Poisson ratio [15]. Plane-wave matrix elements of U and H_{SO} determine the scattering matrix, which can be written in the Born approximation as:

$$\begin{aligned} S(\vec{k}, \vec{k}') &= i(\langle \vec{k}|U|\vec{k}'\rangle + \langle \vec{k}|H_{\mathrm{SO}}|\vec{k}'\rangle) \\ &\equiv g(\vec{k}, \vec{k}') + ih(\vec{k}, \vec{k}')\vec{\sigma} \cdot \hat{n}(\vec{k}, \vec{k}'). \end{aligned} \tag{3}$$

Here $g(\vec{k}, \vec{k}')$ and $h(\vec{k}, \vec{k}')$ are the regular (non-spin-flip) and spin-flip scattering amplitudes, respectively [16,17], and $\hat{n}(\vec{k}, \vec{k}')$ is a unit pseudovector depending on the mutual orientation of the incident wave vector $\vec{k}$, scattered wave vector $\vec{k}'$, and the defect axis z. In the case $\vec{k} \perp z$, $\hat{n}(\vec{k}, \vec{k}')$ is normal to the scattering plane formed by $\vec{k}$ and $\vec{k}'$. For spherical defects, the amplitudes $g(\vec{k}, \vec{k}')$ and $h(\vec{k}, \vec{k}')$ have similar angular dependencies. As a result, the regular scattering amplitude always exceeds the spin-flip amplitude due to the weakness of the spin-orbit coupling. For a nonspherical defect such as the line dipole considered here, however, these quantities have different angular dependencies, and the amplitude for spin-flip scattering can be comparable to or exceed the regular scattering amplitude.

The spin polarization can be calculated from the scattering matrix following Merzbacher [16] and Landau and Lifschitz [17]. We are primarily concerned with electrons moving towards the GaAs quantum well ($\vec{k}||[00\bar{1}]$) and having a large longitudinal component of the initial spin polarization $\vec{P}_0(\vec{k})||\vec{k}$. This corresponds to spin injection across the interface with an out-of-plane applied magnetic field. Calculating the final spin polarization $\vec{P}(\vec{k}')$ of the electron scattered in the direction of $\vec{k}'$, we introduce the function

$$\pi(\vec{k}, \vec{k}') = \frac{1}{2} + \frac{\vec{k}\vec{P}(\vec{k}')}{2\vec{k}\vec{P}_0(\vec{k})} = \frac{1}{2} + \frac{|g(\vec{k}, \vec{k}')|^2 - |h(\vec{k}, \vec{k}')|^2 + 2|h(\vec{k}, \vec{k}')|^2 \vec{k} \cdot \hat{n}(\vec{k}, \vec{k}')/k}{2[|g(\vec{k}, \vec{k}')|^2 + |h(\vec{k}, \vec{k}')|^2]}, \tag{4}$$

describing the angular distribution of the spin polarization. This function is a natural measure of the probability of spin-flip processes. Its value lies between 0 (all spin-flip) and 1 (no spin-flip), with $\pi(\vec{k}, \vec{k}') = 0.5$ corresponding to zero net spin polarization. When $\pi(\vec{k}, \vec{k}')$ is close to zero, the spin-flip processes dominate and result in significant degradation of the spin polarization.

The angular distribution of the spin polarization $\pi(\vec{k}, \vec{k}')$ about the defect axis is presented in Fig. 5 (solid

lines) for electrons incident normal to the interface and for different values of the electron energy expressed as the dimensionless parameter kr_0 ($kr_0 \sim 1$ corresponds to electrons at the Fermi level). The Thomas-Fermi screening distance r_0 is approximately 100 Å for the carrier densities considered experimentally (10^{16}–10^{17} cm^{-3}). The outer dashed circle corresponds to 100% spin polarization (*no* spin-flip scattering), while the origin corresponds to *all* spin-flip scattering (opposite polarization). The inner dashed circle corresponds to zero spin polarization, where one half of the carriers have flipped their spin due to interaction with the defect potential.

The most striking characteristic of the plot is that spin-flip scattering dominates for forward scattering for all electron energies—interaction with the defect potential has a very high probability for spin-flip and results in a significant reduction of the spin polarization when averaged over all the interface sites. Thus, the longitudinal component of the spin polarization of the electrons scattered forward at small angles (towards the GaAs quantum well) will be significantly reduced. While spin-orbit scattering is normally a small effect, it is strongly enhanced due to the nonspherical character of the defect potential. This is due to the fact that the dipole potential Eq. (2) changes its sign under space inversion, and the amplitude $g(\vec{k}, \vec{k}')$ tends to zero while $h(k, k')$ remains finite; i.e., the spin-flip scattering becomes dominant. Qualitatively similar results are obtained for other orientations of the dipole moment.

For direct comparison with experiment, an estimate of the net electron spin polarization in the GaAs quantum well, P_{spin}, can be made for a linear interface defect density n in the dilute limit (single scattering). The preceding analysis has shown that forward scattering due to interaction with the defect potential is clearly accompanied by spin-flip (Fig. 5). Therefore, we adopt a 100% spin-flip for any electron interacting with such a defect, enabling a straightforward estimate of P_{spin}. The spatial extent of the defect potential is approximated by the Thomas-Fermi screening radius, which is $r_o \approx 100$ Å for the electron densities of the ZnMnSe and AlGaAs layers in the spin-LEDs studied (10^{16}–10^{17} cm^{-3}). Thus, *all* electrons crossing the interface within r_o on either side of the defect will be spin-flipped. The spin polarization of the incident current (assumed to be 100% polarized) is reduced by a factor proportional to the defect density n, and P_{spin} is given by

$$P_{\text{spin}} \approx 1 - (2r_o)2n, \tag{5}$$

where the factor of $2n$ accounts for the contribution of the line defects along both [110] and [1$\bar{1}$0]. This calculated behavior is shown as the dashed line in Fig. 3 and shows good agreement with the experimental data with *no* adjustable parameters.

In summary, these results provide the first direct correlation between the spin-injection efficiency across a heteroepitaxial interface and the interface defect structure. The contribution of the nonspherically symmetric defect potential to the spin-orbit coupling results in enhanced spin-flip scattering and a reduction in spin polarization. Because interface defects are generic to heteroepitaxial systems, these results should apply to all spin transport heterostructures.

This work was supported by the Office of Naval Research and the Defense Advanced Research Projects Agency *SpinS* program. Y. D. P. and A. T. H. gratefully acknowledge support from NRL/NRC. A. G. P. gratefully acknowledges financial support from the ASEE-ONR Summer Faculty Program and NSF Grant No. DMR-0071823.

*Current address: School of Physics and CSCMR, Seoul National University, Seoul 151-747, Korea.

†Permanent address: Physics Department, South Dakota School of Mines and Technology, Rapid City, South Dakota 57701.

[1] R. Fiederling *et al.*, Nature (London) **402**, 787 (1999).

[2] B. T. Jonker *et al.*, Phys. Rev. B **62**, 8180 (2000); Y. D. Park *et al.*, Appl. Phys. Lett. **77**, 3989 (2000); B. T. Jonker *et al.*, Appl. Phys. Lett. **79**, 3098 (2001).

[3] Y. Q. Jia, R. C. Shi, and S. Y. Chou, IEEE Trans. Magn. **32**, 4707 (1996); P. R. Hammar *et al.*, Phys. Rev. Lett. **83**, 203 (1999); C.-M. Hu *et al.*, Phys. Rev. B **63**, 125333 (2001); S. Gardelis *et al.*, Phys. Rev. B **60**, 7764 (1999).

[4] H. J. Zhu *et al.*, Phys. Rev. Lett. **87**, 016601 (2001); A. T. Hanbicki *et al.*, Appl. Phys. Lett. **80**, 1240 (2002); V. F. Motsnyi *et al.*, Appl. Phys. Lett. **81**, 265 (2002).

[5] G. Schmidt *et al.*, Phys. Rev. B **62**, R4790 (2000).

[6] J. M. Maclaren, W. H. Butler, and X.-G. Zhang, J. Appl. Phys. **83**, 6521 (1998).

[7] G. A. de Wijs and R. A. de Groot, Phys. Rev. B **64**, 020402(R) (2001); J. T. Olesberg *et al.*, Phys. Rev. B **64**, 201301(R) (2001).

[8] B. T. Jonker, U.S. Patent 5 874 749 (February 23, 1999).

[9] F. Meier and B. P. Zakharchenya, *Optical Orientation* (North-Holland, Amsterdam, 1984), Vol. 8.

[10] K. K. Fung, N. Wang, and I. K. Suo, Appl. Phys. Lett. **71**, 1225 (1997); T. Walter and D. Gerthsen, Ultramicroscopy **81**, 279 (2000).

[11] M. A. Vidal *et al.*, Defect Diffus. Forum **173–174**, 32 (1999).

[12] C. Gianni *et al.*, J. Phys. D **32**, A51 (1999).

[13] M. Oestreich *et al.*, Appl. Phys. Lett. **74**, 1251 (1999).

[14] G. E. Pikus and A. N. Titkov, in *Optical Orientation* (North-Holland, Amsterdam, 1984), p. 73; M. I. D'yakonov *et al.*, Zh. Eksp. Teor. Fiz. **90**, 1123 (1986) [Sov. Phys. JETP **63**, 655 (1986)].

[15] J. S. Koehler, Phys. Rev. **60**, 397 (1941); R. Landauer, Phys. Rev. **82**, 520 (1951); D. L. Dexter, Phys. Rev. **85**, 936 (1952); D. L. Dexter and F. Seitz, Phys. Rev. **86**, 964 (1952).

[16] E. Merzbacher, *Quantum Mechanics* (Wiley, New York, 1998), p. 402.

[17] L. D. Landau and E. M. Lifshitz, *Quantum Mechanics* (Addison-Wesley, Reading, MA, 1958).